AFRL-OSR-VA-TR-2015-0069

FUNCTIONALIZATIONS OF SEMICONDUCTOR NANOMATERIALS FOR OPTOELECTROINC DEVEICE AND

Omar Manasreh
UNIVERSITY OF ARKANSAS

03/04/2015
Final Report

Air Force Research Laboratory
AF Office Of Scientific Research (AFOSR)/ RTD
Arlington, Virginia 22203
Air Force Materiel Command

REPORT DOCUMENTATION PAGE

Form Approved
OMB No. 0704-0188

1. REPORT DATE *(DD-MM-YYYY)*	2. REPORT TYPE	3. DATES COVERED *(From - To)*
11/02/2015	Final	14-04-2011 to 01-08-2014

4. TITLE AND SUBTITLE
Functionalization of semiconductor nanomaterials for optoelectronic devices and components

5a. CONTRACT NUMBER

5b. GRANT NUMBER
FA9550-10-1-0136

5c. PROGRAM ELEMENT NUMBER

6. AUTHOR(S)
Manasreh, Omar

5d. PROJECT NUMBER
FA9550-10-1-0136

5e. TASK NUMBER

5f. WORK UNIT NUMBER

7. PERFORMING ORGANIZATION NAME(S) AND ADDRESS(ES)
University of Arkansas
Department of Electrical Engineering
3217 Bell Engineering Center
Fayetteville, AR 72701

8. PERFORMING ORGANIZATION REPORT NUMBER

9. SPONSORING/MONITORING AGENCY NAME(S) AND ADDRESS(ES)
Air Force Office of Scientific Research
875 N. Randolph Street
Arlington, VA 22203

10. SPONSOR/MONITOR'S ACRONYM(S)
AFOSR

11. SPONSOR/MONITOR'S REPORT NUMBER(S)

12. DISTRIBUTION/AVAILABILITY STATEMENT
Distribution A

13. SUPPLEMENTARY NOTES
None

14. ABSTRACT
Various semiconductor nanomaterials were functionalized for optoelectronic devices, such as photovoltaics and photodetectors. Successful functionalization schemes included: surface modification of GaAs to enhance light absorption; to improve photovoltaic response, application of a MoO3 thin film onto a PbS coupled ZnO nanorod layer; Ag nanoparticles on FeS2; and photodetcors enhanced by addition of nanoparticles. The project concluded having exceeded its proposed objectives.

15. SUBJECT TERMS

16. SECURITY CLASSIFICATION OF:			17. LIMITATION OF ABSTRACT	18. NUMBER OF PAGES	19a. NAME OF RESPONSIBLE PERSON
a. REPORT	b. ABSTRACT	c. THIS PAGE			Kenneth C. Goretta
				17	19b. TELEPHONE NUMBER *(Include area code)* 703 696 7349

INSTRUCTIONS FOR COMPLETING SF 298

1. REPORT DATE. Full publication date, including day, month, if available. Must cite at least the year and be Year 2000 compliant, e.g. 30-06-1998; xx-06-1998; xx-xx-1998.

2. REPORT TYPE. State the type of report, such as final, technical, interim, memorandum, master's thesis, progress, quarterly, research, special, group study, etc.

3. DATE COVERED. Indicate the time during which the work was performed and the report was written, e.g., Jun 1997 - Jun 1998; 1-10 Jun 1996; May - Nov 1998; Nov 1998.

4. TITLE. Enter title and subtitle with volume number and part number, if applicable. On classified documents, enter the title classification in parentheses.

5a. CONTRACT NUMBER. Enter all contract numbers as they appear in the report, e.g. F33315-86-C-5169.

5b. GRANT NUMBER. Enter all grant numbers as they appear in the report. e.g. AFOSR-82-1234.

5c. PROGRAM ELEMENT NUMBER. Enter all program element numbers as they appear in the report, e.g. 61101A.

5e. TASK NUMBER. Enter all task numbers as they appear in the report, e.g. 05; RF0330201; T4112.

5f. WORK UNIT NUMBER. Enter all work unit numbers as they appear in the report, e.g. 001; AFAPL30480105.

6. AUTHOR(S). Enter name(s) of person(s) responsible for writing the report, performing the research, or credited with the content of the report. The form of entry is the last name, first name, middle initial, and additional qualifiers separated by commas, e.g. Smith, Richard, J, Jr.

7. PERFORMING ORGANIZATION NAME(S) AND ADDRESS(ES). Self-explanatory.

8. PERFORMING ORGANIZATION REPORT NUMBER. Enter all unique alphanumeric report numbers assigned by the performing organization, e.g. BRL-1234; AFWL-TR-85-4017-Vol-21-PT-2.

9. SPONSORING/MONITORING AGENCY NAME(S) AND ADDRESS(ES). Enter the name and address of the organization(s) financially responsible for and monitoring the work.

10. SPONSOR/MONITOR'S ACRONYM(S). Enter, if available, e.g. BRL, ARDEC, NADC.

11. SPONSOR/MONITOR'S REPORT NUMBER(S). Enter report number as assigned by the sponsoring/ monitoring agency, if available, e.g. BRL-TR-829; -215.

12. DISTRIBUTION/AVAILABILITY STATEMENT. Use agency-mandated availability statements to indicate the public availability or distribution limitations of the report. If additional limitations/ restrictions or special markings are indicated, follow agency authorization procedures, e.g. RD/FRD, PROPIN, ITAR, etc. Include copyright information.

13. SUPPLEMENTARY NOTES. Enter information not included elsewhere such as: prepared in cooperation with; translation of; report supersedes; old edition number, etc.

14. ABSTRACT. A brief (approximately 200 words) factual summary of the most significant information.

15. SUBJECT TERMS. Key words or phrases identifying major concepts in the report.

16. SECURITY CLASSIFICATION. Enter security classification in accordance with security classification regulations, e.g. U, C, S, etc. If this form contains classified information, stamp classification level on the top and bottom of this page.

17. LIMITATION OF ABSTRACT. This block must be completed to assign a distribution limitation to the abstract. Enter UU (Unclassified Unlimited) or SAR (Same as Report). An entry in this block is necessary if the abstract is to be limited.

AFOSR Final report, August 2014

Title: Functionalization of semiconductor nanomaterials for optoelectronic devices and components.

Award No. FA9550-10-1-0136

Program managers: Dr. Gernot Pomrenke.

PI: Omar Manasreh
3217 Bell Engineering Center, Department of Electrical Engineering, University of Arkansas, Fayetteville, AR 72701. Email: manasreh@uark.edu phones: (479)575-6053, cell: (479)966-5965.

The Subject grant is used in support of the following group members:

1. Omar Manasreh, PI
2. Scott Little, Postdoctoral
3. Mahmood Khan, Postdoctoral
4. Yahia Makembleh (PhD Candidate)
5. Jony Sarker (M.S. candidate)
6. Amhed Nusir (M.S. candidate)
7. Scott Mangham, M.S. May 2013
8. Ramesh Vasan, (PhD Candidate).
9. Seungyong Lee, (PhD pAndidate).
10. Juan Aguilar (PhD Candidate)
11. Zack Bever (B.S. graduated)

Publications resulted from the grant:

1. "*Large enhancement in the power conversion efficiency of InAs quantum dot solar cell by using a single layer anatase TiO_2 anti-reflection coating*," R. Vasan, Y. F. Makableh, J. C. Sarker, and M. O. Manasreh, IEEE Electron Device Letters. (Submitted).
2. "*Broadband Nanostructured Antireflection Coating for Enhancing InAs/GaAs Quantum Dots Solar Cells Performance*," J. C. Sarker, Y. F. Makableh, R. Vasan, S. Lee, M. O. Manasreh, and M. Benamara, IEEE J. Photovoltaic. (submitted).
3. "*Synthesis, characterization and optoelectronic properties of iron pyrite nanohusks*," M. Alam Khan, M. O. Manasreh, and Yong-Mook Kang, Materials Letters **126**, 181-184 (2014). http://dx.doi.org/10.1016/j.matlet.2014.04.060
4. "*Enhanced performance of surface modified InAs quantum dots solar cell by sol-gel grown tantalum pentoxide antireflection coating*," J. C. Sarker, R. Vasan,Y. F. Makableh, S. Lee, A. I. Nusir, and M. O. Manasreh, J. Solar Energy Materials and Solar Cells **127**, 58-62 (2014). http://dx.doi.org/10.1016/j.solmat.2014.03.055
5. "Enhancement of GaAs solar cell performance by using a ZnO sol-gel anti-reflection coating," Y. F. Makableh*, R. Vasan, J. C. Sarker, A. I. Nusir, S. Seal, and M. O. Manasreh,

J. Solar Energy Matarials and Solar Cells. 123, 178-182 (2014). http://dx.doi.org/10.1016/j.solmat.2014.01.007

6. "*Uncooled photodetector based on CdSe nanocrystlas with an interdigital metallization*," A. I. Nusir, J. Aguilar, Z. Bever, and M. O. Manasreh, Appl. Phys. Lett. **104**, 051124 (2014). http://dx.doi.org/10.1063/1.4864636

7. *"Enhanced Response in InAs Quantum Dot in a Quantum Well Solar Cells by Using Poly-L-lysine Homopolymers*," Y. F. Makableh, R. Vasan, S. Lee, M. Alam Khan, and M. O. Manasreh, Materials Research Society, Symp. Proc. Volume 1551 (2013). http://dx.doi.org/10.1557/opl.2013.966

8. "*Enhanced Photocurrent due to Interband Transitions from InAs Quantum Dots Embedded in InGaAs Quantum Well Solar Cells*," R. Vasan, Y. F. Makableh, J. C. Sarker, and M. O. Manasreh, Materials Research Society, Mater. Res. Soc. Symp. Proc. Vol. 1551 (2013). http://dx.doi.org/10.1557//opl.2013.742

9. "*The Optimization of InP/ZnS Core/Shell Nanocrystals and TiO_2 Nanotubes for Quantum Dot Sensitized Solar Cells*," Seungyong Lee, Rick Eyi, Mahmood Khan, Scott Little, M. O. Manasreh, Materials Research Society, Mater. Res. Soc. Symp. Proc. Vol. 1578 (2013). http://dx.doi.org/10.1557//opl.2013.984

10. "*Colloidal growth, characterization and optoelectronic study of strong light absorbent inexpensive iron pyrite nanomaterials by using amine ligands for photovoltaics application*," M. Alam Khan, Scott A. Little, Y. Makablah, Scott Mangham, S.Y. Lee and M. O. Manasreh, Materials Research Society, Mater. Res. Soc. Symp. Proc. Vol. 1545 (2013). http://dx.doi.org/10.1557/opl.2013.957

11. "*Processing of pristine single and multiwalled carbon nanotubes as different stacking layers in bulk heterojunction solar cells*," M. Alam Khan, Michio Matsumura and M. O. Manasreh, Materials Research Society, Spring 2013, Symposium B, San Francisco, April 1-5. (Accepted).

12. "*Enhancement of the performance of InAs quantum dots solar cell by surface modification using Poly-L-Lysine homopolymers*," Y. F. Makableh, R. Vasan, S. Lee, and O. M. Manasreh, Appl. Phys. Lett. **102**, 051904 (2013). http://dx.doi.org/10.1063/1.4789908

13. *"Synthesis of iron pyrite nanocrystals utilizing trioctylphosphine oxide (TOPO) for photovoltaic devices*," S. C. Mangham, M. A. Kahn, M. Benamara, M. O. Manasreh, Materials Letters **97**, 144-147 (2013). http://dx.doi.org/10.1016/j.matlet.2013.01.101

14. "*Colloidal $Cu(In_xGa_{1-x})Se_2$ nanocrystals for all-inorganic nanocomposite solar cells*," Vanga R. Reddy, Jiang Wu, and M. O. Manasreh, Materials Letters **92**, 296-299 (2013). http://dx.doi.org/10.1016/j.matlet.2012.10.097

15. *"Colloidal $CuInS_2$ Based Nanocrystals/TiO_2 Nanotubes Arrays Composite Solar Cells Fabrication and Testing,"* Vanga Reddy, William Wilson, Rick Eyi, Jiang Wu, Scott Mangham, Omar Manasreh, John Dixion and Andrew Wang, in Symposium CC: Functional Semiconductor Nanocrystals and Metal-Hybrid Structures, Mater. Res. Soc. Symp. Proc. vol. **1409** (2012). http://dx.doi.org/10.1557/opl.2012.729

16. *"Synthesis of Colloidal InP/ZnS Nanocrystals for a Photosensitizer,"* Seungyong Lee, Vanga

R. Reddy, Jiang Wu, Rick Eyi and Omar Manasreh, in Symposium CC: Functional Semiconductor Nanocrystals and Metal-Hybrid Structures, Mater. Res. Soc. Symp. Proc. vol. **1409** (2012). http://dx.doi.org/10.1557/opl.2012.778

17. *"Surface Plasmon Enhanced Photoluminescence in InAs Quantum Dots by Spherical Ag Nanoparticles,"* Scott C. Mangham, Jiang Wu, Seungyong Lee, Vanga R. Reddy and Omar Manasreh, in Symposium J: Photonic and Plasmonic Materials for Enhanced Photovoltaic Performance, Mater. Res. Soc. Symp. Proc. vol. **1391** (2012). http://dx.doi.org/10.1557/opl.2012.692

18. *"Localized Surface Plasmon Enhanced Quantum Dot Solar Cells,"* Jiang Wu, Scott Mangham, Rick Eyi, Seungyong Lee, Vanga R. Reddy and Omar Manasreh, in Symposium J: Photonic and Plasmonic Materials for Enhanced Photovoltaic Performance, Mater. Res. Soc. Symp. Proc. vol. **1391** (2012).

    http://dx.doi.org/10.1557/opl.2012.1213

19. *"Intermediate band solar cells based on InAs quantum dots embedded in* $In_xGa_{1-x}As$ *quantum wells,"* Y. M. F. Makableh, R. Vasan, M. O. Manasreh, IEEE Electron Device Letters (Submitted).

20. *"Characteristics of p-ZnO/n-GaN heterojunction photodetector,"* Abla Al-Zouhbi, N. S. Al-Din, M. O. Manasreh, Optical Review **19** (4), 235-237 (2012). http://dx.doi.org/10.1007/s10043-012-0035-5

21. "*Surface plasmon enhanced intermediate band based quantum dots solar cells*," Jiang Wu, S. Mangham, V. Reddy, M. O. Manasreh, and B. D. Weaver, Solar Energy Materials and Solar Cells **102**, 44-49 (2012). http://dx.doi.org/10.1016/j.solmat.2012.03.032

22. "*Strong interband transitions in InAs quantum dots solar cell*," Jiang Wu, Y. F. M. Makableh, R. Vasan, M. O. Manasreh, B. Liang, C. J. Reyner, and D. L. Huffaker, Appl. Phys. Lett. **100**, 051907, (2012). http://dx.doi.org/10.1063/1.3681360

23. "*Influence of template type and buffer strain on structural properties of GaN multilayer quantum wells grown by PAMBE, an x-ray study*," V. P. Kladko, A. V. Kuchuk, N. V. Safryuk, V. F. Machulin, P. M. Lytvyn, V. G. Raicheva, A. E. Belyaev, Yu. I. Mazur, E. A. DeCuir, Jr.; M. E. Ware, M. O. Manasreh, G. J. Salamo, Journal of Physics D 44, 025403-8 (2011). http://dx.doi.org/10.1088/0022-3727/44/2/025403

24. "*System for spectral Characterization of Solar Cell Structures*," R. Ciocan, D. Han, D. Assalone, Z. Li, E. Ciocan, M. Lloyd, T. Moriarty, K. Emery, J. Wu, S. Lee, S. Mangham, R. Vanga, M. O. Manasreh, Photovoltaic Specialists Conference (PVSC), 2011 37th IEEE. 001734–001738 (2011). http://dx.doi.org/10.1109/PVSC.2011.6186289

25. "*Photoluminescence plasmonic enhancement in InAs quantum dots coupled to gold nanoparticles*," Jiang Wu, Seungyong Lee, V. R. Reddy, M. O. Manasreh, B. D. Weaver, M. K. Yakes, C. S. Furrow, Vas. P. Kunets, M. Benamara, and G. J. Salamo, Materials Letters **65**, 3605-3608 (2011). http://dx.doi.org/10.1016/j.matlet.2011.08.019

I. Introduction

The funding from the AOFSR and the cost sharing form the University of Arkansas were used to investigate various semiconductor nanomaterials and functionalize them for optoelectronic devices, such as photovoltaic and photodetectors. The description below is a brief details about the recent work performed under the subject grant.

A. **Surface modification of GaAs**:

Light absorption enhancement due to surface modification on GaAs solar cell has been investigated. The solar cells were fabricated in a class 100 clean room using established photolithography procedures. The solar cells surface modification was performed using two anti-reflection coatings (ARC) schemes. In the first scheme one layer anti-reflection coating is used. In the second scheme two layers will be used. For the purpose of using single layer or for the first layer coating, materials with refractive index on the order of 2.0 have to be used, such as ZnO, and ZnS. While for the second layer materials with refractive index on the order of 1.4 will be used such as MgF_2 and SiO_2. Moreover, SiO2 nanoparticles are under investigation for ARC coating purpose, and for obtaining self-cleaning surface properties as well.

The material fabrication was performed in tow techniques: First, ebeam deposition was used to deposit MgF_2. Second, sol-gel chemical base method was used for all other materials. Spin coating method was used to apply the sol-gel based materials on several solar cell devices. The sol-gel layers where characterized using micro-Raman spectroscopy as shown in **Fig. 1**. Transmission spectra were reordered for the different ARC coatings on GaAs for the optimization process. Current-Voltage characteristics were performed for the solar cells before and after applying the ARC to investigate their effect of on the solar cells.

The spin coating process of the sol-gels was done using different speeds to optimize for the best device efficiency enhancement. The speeds were varied between 2000 rpm – 12000 rpm in a 1000 rpm steps, for 30 seconds. The process was repeated for each material to get the best device enhancement. It has been found that for the higher refractive index materials a spin coating speed around 8000 rpm can give the best enhancement, but for the lower refractive index materials lower speeds as 5000 rpm can give optimum results. The transmission spectra obtained for the best GaAs samples coated with ARC materials are shown in **Fig. 2**.

The IV characteristics obtained before and

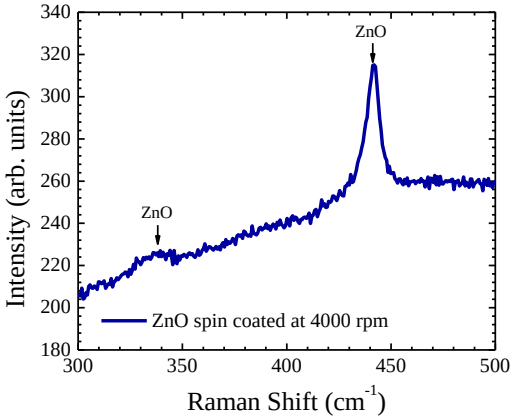

Fig. 1. *Raman spectra of ZnO sol-gel spin coated at 4000 rpm, and annealed at 150 ^oC*

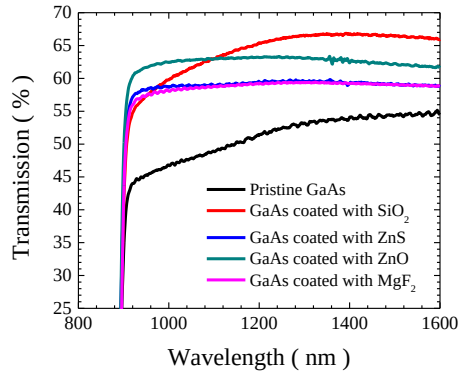

Fig. 2. *Transmission spectra of ARC materials coated on semi insulating GaAs samples.*

after the application of the ARC on the solar cell. Results obtained for reference solar cells are shown in **Fig. 3**.

The enhancement seen in the power conversion efficiency is on the order of 35 %. The enhancement noticed from the MgF_2 and SiO_2 were in the 25 % range, which is expected as being lower refractive index materials. This improvement was observed in the photocurrent, with no change in the open circuit voltage. Since no change noted in the filling factor or the open circuit voltage, the enhancement in the short current density and the power conversion efficiency is related to the ARC effect, in which enhanced the photon absorption in the device active region.

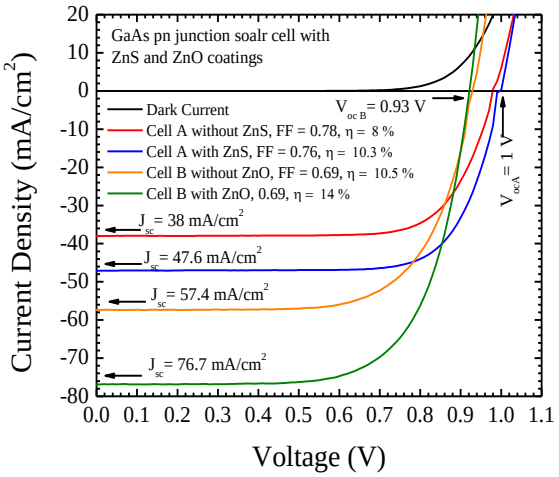

Fig. 3. *The IV characteristics of the GaAs solar cell before and after ZnO and ZnS coating.*

To further investigate the properties of the SiO_2 nanoparticles, three nanoparticles sizes were used 60, 20 and 7 nm nanoparticles. The 60 nm nanoparticles were synthesized using the sol-gel method, while the other two sizes were obtained from Sigma Aldrich. The deposition of these nanoparticles is done using immersing method in the nanoparticles solutions. The immersion process optimization is done through changing the time of immersion and the density of the particles in the solution. Scanning electron microscopy was used to test the samples after coupling the nanoparticles to the surface, as shown in **Fig. 4**. The work on the nanoparticles deposition and characterization of the nanoparticles still under progress.

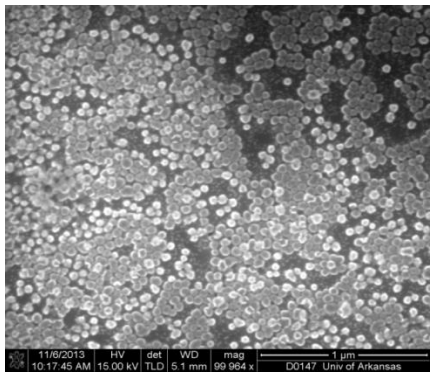

Fig. 4. *Silicon dioxide nanoparticles coupled to GaAs surface*

Device performance enhancement due to anti-reflection coating was investigated on GaAs solar cells using ZnO, ZnS, MgF_2 and SiO_2 materials. The single layer ARC optimization followed the refractive index matching for optimum region for GaAs solar cells according to the equation ($n_{ARC} = \sqrt{n_o n_{GaAs}}$), where n_o = 1 is the air refractive index. Second layer ARC optimization is under investigation. The SiO_2 nanoparticles will be modified to work as ARC and self-cleaning surface at the same time.

B. **ZnO nanorod based PbS nanocrystal solar cells:**

PbS nanocrystals were synthesized using lead oxide and bis(trimethylsilyl)sulfide. The absorption spectrum is displayed in **Fig. 1**. The lead and sulfur precursors readily react each other and easily form particles. PbS nanocrystals are synthesized through nucleation and subsequent particle growth. Stabilizing ligand and solvent are key factors that lead to narrow size distribution and well dispersed nanocrystals in a solvent. Oleic acid as a ligand was used and

served well in this capacity. Oleic acid has also an effect on the reactivity of monomer. With the high concentration of oleic acid, the size of PbS nanocrystals is broad, presumably due to a lack of a discrete nucleation event that results in uncontrolled growth onto fewer nuclei. When bis(trimethylsilyl)sulfide is used as a sulfur precursor, the success of narrow dispersed PbS nanocrystals is achieved in high concentration of oleic acid because of increased reactivity of the bis(trimethylsilyl)sulfide precursor compared to the elemental sulfur. For the synthesis of PbS, a ratio 10:2:1 of oleic acid/Pb/S was adopted.

Upon the injection of bis(trimethylsilyl)-sulfide into Pb precursor dissolved in oleic acid, the color of the reaction mixture was drastically changed from yellow to dark brown in a few seconds. Heating the reaction mixture promotes particle growth, evidenced by a gradual red shift with increased growth time at elevated temperatures. The PbS nanocrystals grown for 8 minutes at 100 ℃ have an absorption peak at 1400 nm in wavelength shown in **Fig. 1**. The average size of the PbS nanocrystals is estimated to be 6 nm in diameter from the absorption peak. The shape of PbS nanocrystals is dominated by kinetics. By modifying reaction parameters the PbS particles are observed to vary widely from bent rod-like particles to star-like polyhedrons. Particles removed from the reaction shortly after injection appear strongly angular and faceted, indicating particle growth occurs along preferred crystal directions. Prolonged heating gives rise to smooth shape of nanocrystals by the decreased number of sharp edges on the particles. By varying the injection temperature and the ratio of ligand to the Pb/S precursor, the shape can also be tuned from nearly spherically shaped tetradecahedrons to almost cubic.

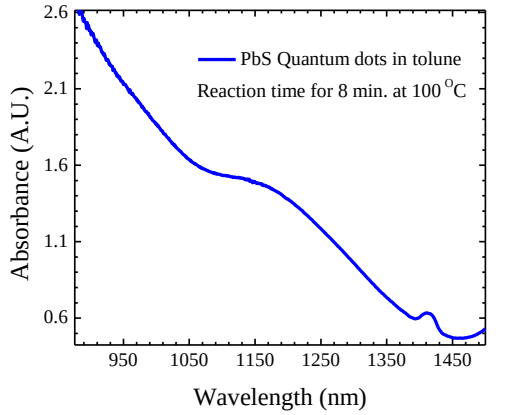

Fig. 1. *Absorption spectrum of PbS nanocrystals synthesized for 8 min at 100 ℃ shows a peak at wavelength of 1400 nm.*

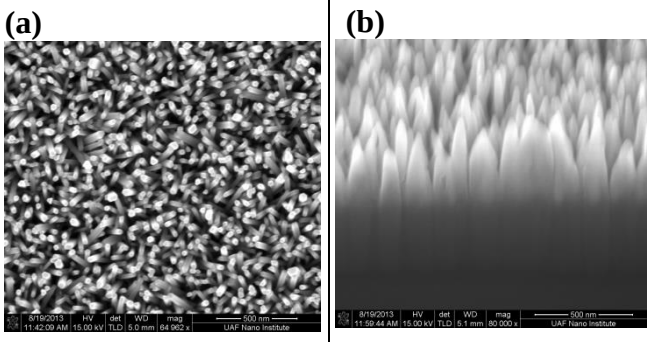

Fig. 2. *(a) Plan-view SEM image shows ZnO nanorod grown on seed layers. (b) Tilted SEM image of ZnO nanorods shows the diameter and the length of the nanorods.*

In order to couple with the synthesized PbS nanocrystals for photovoltaic applications, ZnO nanorod arrays were grown on a sol-gel ZnO seed layer by hydrothermal growth technique. To prepare a sol-gel precursor for a seed layer, solutions of zinc acetate dehydrate and ethanolamine in 2-methoxyethanol were mixed in equal proportion. This mixture was then spin casted and annealed in air to form a uniform and complete film. ZnO nanorods were grown on the ZnO seed layer, floating facedown in an aqueous container containing equal volumes of zinc nitrate hexahydrate and hexamethylenetetramine in deionized water at elevated temperature. The length and the diameter of the ZnO nanorods can be

controlled by main parameters such as temperature, growth time, and concentration of the solution. SEM images of the ZnO nanorodes are shown in **Fig. 2**.

In order to obtain an efficient hole extraction from the PbS layer, MoO_3 thin film, as a hole injection layer was spin casted on the PbS coupled ZnO nanorod layer. Solution-processed MoO_3 was prepared by reacting MoO_3 powder with H_2O_2 in a reflux system for 2 hours at 80 ℃ in air. Then the solution was cooled down to room temperature for 24 hours to obtain a clear yellow liquid. The viscosity and concentration of the solution were further adjusted with the addition of polyethylene glycol and 2-methoxyethanol. This solution-processed MoO_3 does not require ligands for nanoparticle stabilization and thus have a good carrier transport property without the need to remove electrically insulating ligands through a post synthesis step.

The ZnO nanorods based Bulk heterojunction PbS solar cell was fabricated shown in **Fig. 3 (a)**. MoO_3 layer was deposited to improve solar cell efficiency by enhancing hole extraction from the active layer. The fabricated device achieved photocurrents of 0.1 mA/cm^2 and open circuit voltage of 0.12 V shown in **Fig. 3 (b)**. The efficiency and fill factor of the device were 0.35 % and 0.28, respectively. For further enhancement of the solar cell performance, The MoO_3 interlayer eliminates the Schottky barrier and improves all photovoltaic performance but does not seem to be a good physical buffer layer against shorting between the ZnO nanorods and the top metal electrode.

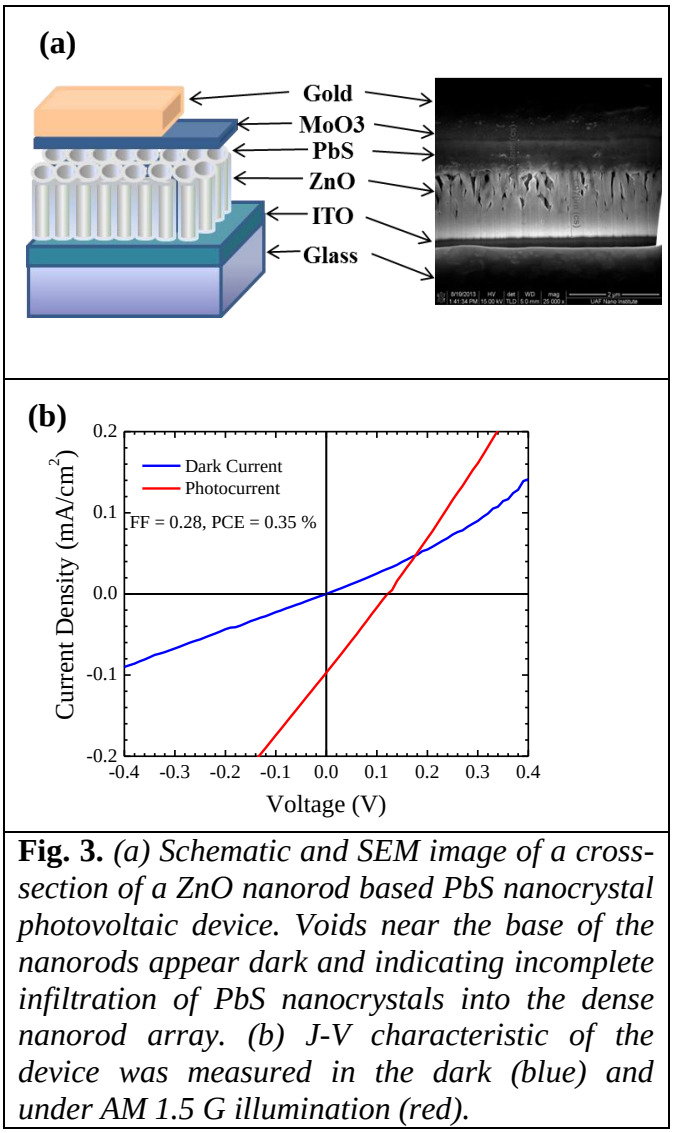

Fig. 3. *(a) Schematic and SEM image of a cross-section of a ZnO nanorod based PbS nanocrystal photovoltaic device. Voids near the base of the nanorods appear dark and indicating incomplete infiltration of PbS nanocrystals into the dense nanorod array. (b) J-V characteristic of the device was measured in the dark (blue) and under AM 1.5 G illumination (red).*

C. **Iron Pyrite**:

Recently, the group has been working on synthesis of FeS_2 or iron pyrite nanocrystals. The goal is to make iron pyrite thins film that will be used later on as photo active layers. Iron pyrite has been investigated as a photoactive material because of its high absorption coefficient, less than 200 nm of FeS_2 thin film is able to absorb 90% of visible light. Iron pyrite, as the most abundant metal sulfur of the earth crust is inexpensive. Even though it has been investigated for more than a decade, researchers still find it difficult to observe a good photoconductivity in FeS_2 optoelectronics devices. The problem stem from the fact that there are many materials with different sulfur to iron ratios, FeS, Fe_3S_4, FeS_6 and there is even another phase of the FeS_2, called

the marcasite phase. It is really difficult to synthesize pure pyrite structure and even a small percent of the others phases is detrimental for the device performances. It is then crucial to synthesize pure pyrite or cubic phase FeS_2. The synthesis was done using a hot injection and heat up techniques. Two solutions were prepared in two three-neck flask. In the first flask, Iron chloride was dissolved in an amine solution, oleylamine, hexadecylamine, or octadecylamine. In the second flask elemental sulfur is dissolved in either Diphenyl ether or oleylamine. Both solution were degas at 120 C under nitrogen atmosphere for 1 hour. After that either solution 2 is injected directly in solution one and then the temperature is raised to 220 C or the temperature is first raised and the solution 2 is injected after. The heat up method lead to cubic shape iron pyrite nanocrystal, while the hot injection one leads to spherical like nanocrystals. The heat up can also resulted in cubic nanocrystals if some surfactants are added to the mixed. Figure 1 shows an absorbance spectrum of a solution of iron pyrite nanocrystals in chloroform. The nanoparticles were synthesized using the hot injection method, oleylamine was used for the iron precursor and Diphenyl ether for the sulfur precursor. This is a typical absorbance spectrum of iron pyrite nanoparticles.

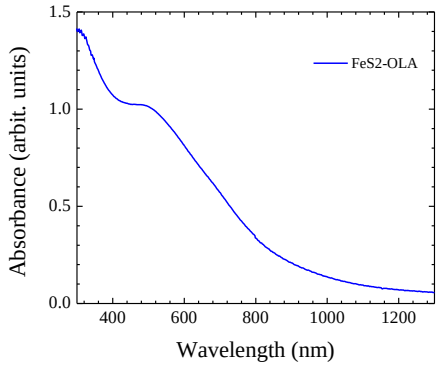

Fig. 1: *Absorption spectrum of Iron pyrite nanoparticles in chloroform*

One other problem associated with iron pyrite apart from the difficulty to synthesize pure cubic phase nanoparticles is films made using these particles tend to lose sulfur other time and this is not good for the stability of the films and the possible optoelectronic devices. One way to solve this issue is to do a surface passivation. The surface passivation was done using ligand exchange. The original amine ligands were replaced by three different ligands, Sb, Fe and $(NH_4)_2S$. These ligands are also shorter compared to the amines. The short length of the ligands will help decrease the interspacing distance between the nanoparticles, which is preferable in order to enhance the electrical conductivity. The absorption spectra of the nanoparticles after ligand exchange were measured along with the Raman spectra to ensure that they remain pyrite, the results are

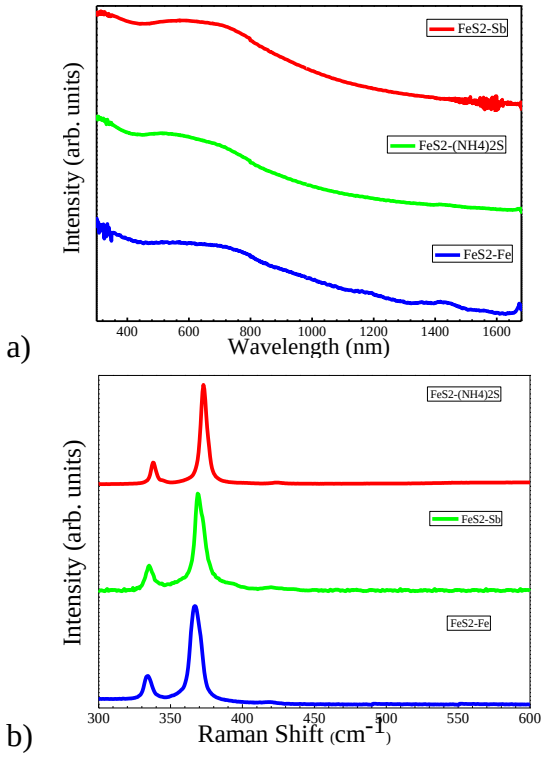

Fig. 2: *FeS_2 nanoparticles after ligand Fe, Sb and $(NH_4)_2S$ ligand exchange, a) absorption spectra and b) Raman spectra*

presented in figured 3. The absorption spectra are very similar, the only difference is the presence of a small shoulder around 1400 nm for the sample with the Fe ligands. The Raman spectra also are those of the pyrite, there are small shift of the Raman peaks.

One other way to prevent a material to change phase is to attach it or linked it to another one and sometimes the connection between the two prevents the first one from changing phase and to stabilize. The connection of the iron pyrite nanoparticles and the metal nanoparticles is under investigation. If this works it could serve as both stabilizer and enhancer of optical properties due to the plasmonic effects. Some researchers have seen decrease in photocurrent were the metallic particles act as traps for the photogenerated carriers. The idea here is to see if in the case of iron pyrite, the good things (phase stability and plasmonic effects) outweigh the possible bad ones (traps). Silver nanoparticles were synthesized for that purpose, the absorption spectrum of the silver nanoparticles in toluene is presented in Figure 3.

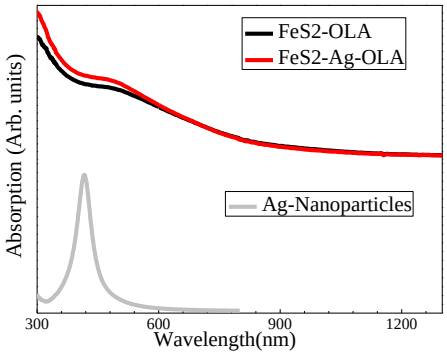

Fig. 3: Absorption spectra of FeS_2, FeS2-Ag and silver nanoparticles in toluene

An attempt to couple metal particles with iron pyrite was done but the effects are still being investigated and so far no change has been observed.

D. **Photodetectors:**

Semiconductor nanocrystals were investigated for a wide range of optoelectronics devices, such as, solar cell and photodetectors. Nanocrystals are grown by wet chemical synthesis, which offers a way for tuning the bandgap by controlling the size of the nanocrystals. Furthermore, the nanocrystals can be dispersed and processed in a solution making them suitable for cost effective mass production. Photodetectors based on nanocrystals are able to operate at room temperature, and detect normal incident light unlike quantum wells. Detection of light in the visible-near-infrared spectral region is important because of many applications based on it. Cadmium selenide (CdSe) nanocrystals with a bandgap of 1.7 eV (730 nm) were implemented in various applications that operate in the visible spectral region 475 – 650 nm. By tuning the bandgap of CdSe nanocrystals it is possible to detect low energy light up to 730 nm wavelength using CdSe nanocrystals. The integration of the nanocrystals with interdigital metallization is expected to simplify the device structure. And improve on its performance by reducing the dark current and increasing the photocurrent.

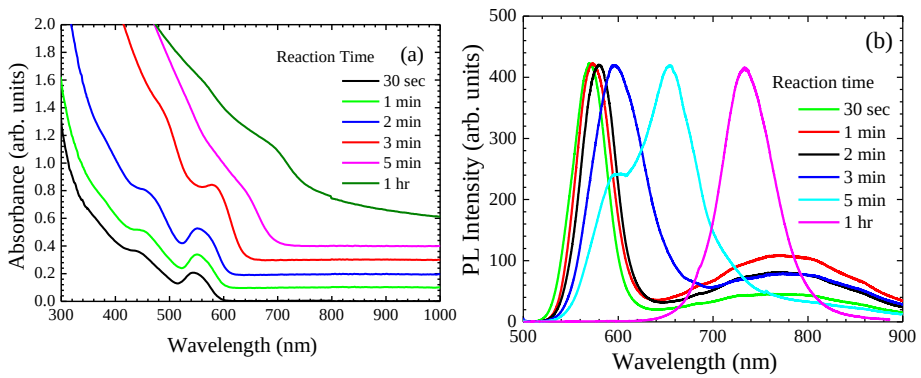

Fig. 1. *(a) Absorbance and (b) PL spectra of the CdSe nanocrystals at*

The absorbance and the photoluminescence (PL) spectra of the nanocrystals are plotted as a function of the growth reaction time in Fig. 1(a) and (b), respectively. The absorbance spectra were measured for the nanocrystals while dispersed in chloroform and placed in a cuvette. The PL spectra were measured for nanocrystals placed on a glass slide after evaporating the solvent (chloroform). The growth reaction time was varied between 30 seconds and one hour. An increase in the growth reaction time beyond an hour does not produce nanocrystals with bandgaps lower than 1.7 eV (730 nm). For one hour reaction time the position of the PL peak was shifted to 730 nm wavelength as shown in Fig. 1

different reaction times

(b). The PL spectrum for an hour reaction time consists of a single narrow peak, which indicates that the size variation is minimized. It is noted that the PL spectrum for the 5 minutes consists of two peaks, which results from the presence of two dominant sizes for the nanocrystals. For shorter reaction times (< 3 min) the broad peak above 650 nm in the PL spectra is a result of unstable state in the nucleation stage.

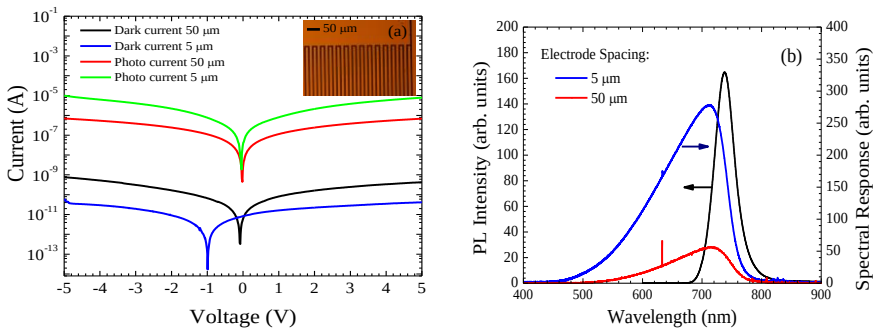

Fig. 2 *(a) I-V characteristics for devices with 5 and 50 μm electrode spacing in dark and under illumination. (b) Spectral response and PL spectra of the devices.*

The current-voltage (I-V) characteristics for the CdSe photodetector with two different electrode spacing (5 and 50 μm) are plotted in Fig. 2 (a). The dark current of the device with 50 μm electrode spacing was 0.25 nA at a bias voltage of 3 V (600 V/cm), whereas the photocurrent was 0.4 μA. By reducing the electrode spacing to 5 μm, the dark current was dropped to 28 pA and the photocurrent was increased to 3.8 μA at 3 V (6,000 V/cm) applied bias. As can be seen in Fig. 2 (a), the photocurrent was about five orders of magnitude higher than the dark current. The inset in Fig. 2 (a) is an image of the templates with an electrodes spacing of 5 μm. The spectral response spectra were measured for the two devices at a bias voltage of 5 V and plotted in Fig. 2 (b). Higher spectral response intensity was obtained from the device with 5 μm electrode spacing compared with the 50 μm spacing device. Due to the increases in photoconductive gain, which depends on the ratio of carrier life time to the carrier transit time.

CdSe nanocrystals were grown by using wet chemical method and characterized by using the optical absorption and PL techniques. Several spectra were collected for nanocrystals grown at different synthesis time. Photodetectors were fabricated from these nanocrystals by spin-coating them on templates with interdigital metallization. The I-V characteristics and spectral response spectra were measured for two devices with interdigital spacing of 5 and 50 μm. It was observed that the device with 5 μm spacing has a superior performance as compared to that with 50 μm spacing.

E. **Zinc oxide nano-rods based glucose biosensors:**

ZnO nano-rods are synthesized on ITO substrate using the hydrothermal growth technique. Optical properties of the ZnO nano-rods have been characterized using UV-visible spectroscopy, raman spectroscopy and the scanning electron microscopy. The band gap of the ZnO nano-rods is found to be approximately 3.54 eV where the increase in the band gap is due to the ZnO nano-rods structure and its surface morphology. Studies from the raman spectroscopy indicate that the rods like ZnO nanostructures have highly crystalline nature. The scanning electron microscopy show that the ZnO nano-rods are ~1.5 microns in length and ~70 nm in diameter. Schematic design for an electrochemical glucose detecting bio-sensor based on aligned ZnO nano-rods has been explained.

Zinc oxide (ZnO) is a bio-compatible, bio-degradable and bio safe material that has emerged as a worldwide research topic especially for medical applications. ZnO is a transparent, wide band-gap direct semiconductor (3.37 eV), with a high exciton binding energy (60 meV) that is widely used in major applications like fabrication of light emitting diodes, ultraviolet lasers, solar cells, etc. ZnO has piezoelectric and pyroelectric properties are being used for manufacturing sensors, transducers and energy generators. In the recent years, one dimensional (1D) nanostructures have played an important role in nano-science technology and research. ZnO NSs and thin-films have gained much attention due to bio-compatible and bio-safe properties that make such materials highly reliable and trustworthy in biomedical science and engineering applications. Among various nanostructure (NS) fabrication methods, the hydrothermal growth technique is a chemical method to synthesize ZnO nano-rods (NRs). This is the most simple, cost effective and low temperature growth process.

Preparation of ZnO sol-gel: The ZnO sol-gel is prepared using zinc acetate dehydrate [Zn $(CH_3COOH)_2 \bullet 2H_2O$, 0.5M] as a precursor dissolved in 10ml of mono-ethanolamine. The solution is stirred at 75℃ and 400 RPM for 1 hour. Next, 0.3 ml of ethanolamine (0.5 M) is added to prepare the sol-gel solution. This sol-gel is spin coated on the ITO coated glass substrate at 4000 rpm for 30 seconds. The substrate is annealed at 180^0C for 2 minutes and another layer is deposited. After spin-coating twice, a thin-film seed layer of ZnO is formed on the substrate that is annealed at 300℃ for 30 minutes in vacuum.

Hydrothermal growth synthesis: The ZnO NR growth solution is prepared using zinc nitrate hexahydrate [Zn (NO3)2·6H2O, 0.05 M] dissolved in 10 ml of de-ionized (DI) water, and hexamethylenetetramine (HMTA) [0.05 M] dissolved in 10 ml of deionized water, stirred individually for an hour. Next, both of these solutions are mixed and stirred for an hour to prepare the final growth solution for the ZnO NRs. The substrate with ZnO thin-film seed layer, is then immersed in the growth solution inside a closed box furnace at 93℃ for 6 hours. The surface of the substrate is washed carefully with DI water to remove solid ZnO power and then dried using nitrogen (N_2) gas.

Characterization: The characterization is done using the absorbance spectroscopy in the range from 200 - 800 nm. Raman spectroscopy is employed to determine the crystallinity of the ZnO thin-film seed layer. Also, the scanning electron microscopy (SEM) is used to scan the sample and produce images showing the distribution and alignment of the ZnO NRs grown.

Raman spectroscopy is a method that can be used to determine the quality and crystallinity of semiconductor nanostructures. **Figure 1** depicts Raman spectrum of hydrothermally synthesized ZnO NRs, where a strong raman active phonon band at 450 cm $^{-1}$ is observed. High crystalline nature of the ZnO NRs is indicated by the presence of an intense peak (also called the E_2 high mode).

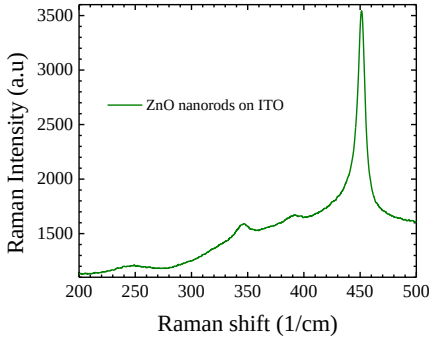

Fig 1: Micro-raman spectroscopy with most dominant peak at 450cm^{-1}

The absorption spectrum in **Fig. 2** depicts that the ZnO NRs have excellent optical quality and exhibit very strong UV emission at ~350 nm. There is a blue shift of 18nm in the in the absorbance spectrum of ZnO NRs when compared to bulk ZnO. Increase in the bandgap is mainly due to the hexagonal surface morphology of the attached nano-rods. **Figure 3** shows the top-down view and the cross-sectional view of SEM images for ZnO nano-rods grown in a closed furnace at an optimized temperature of 93^{0}C for a growth time of 6 hours. The approximate length of these nano-rods is ~1.52 microns while the diameter is ~70 nm. From the SEM images it can be seen that the nano-rods are continuously distributed along the ITO surface.

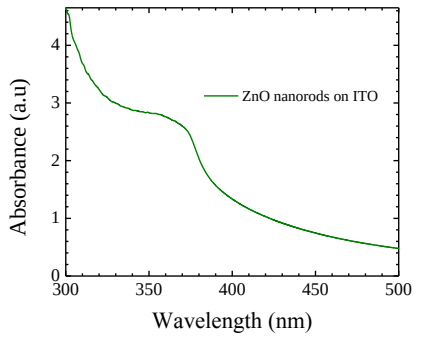

Fig 2: Absorbance spectrum with peak at ~350 nm

After the *vertically aligned ZnO NRs* are grown on ITO, the biosensor unit is fabricated and tested. **Figure 4** shows a three-dimensional representation of glucose detecting biosensor. Immobilized glucose oxidase (GOx) is physically adsorbed and attached to the NRs grown on ITO substrate. Nafion film is then spin coated on the NRs to stabilize the GOx, which prevents enzyme leakage. This ZnO biosensor unit is then immersed into the test cell as shown in figure 5.

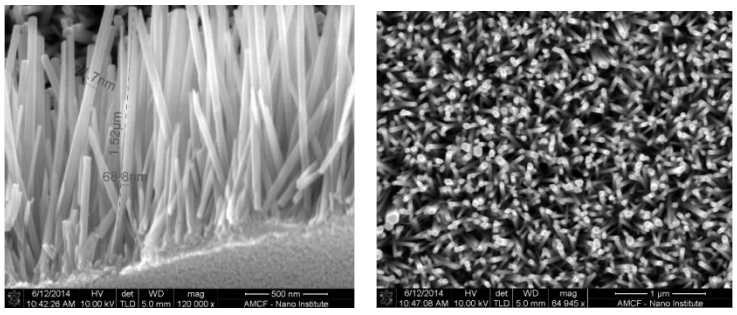

Fig 3: *Scanning Electron Microscopy images of ZnO NRs grown on ITO substrate.*

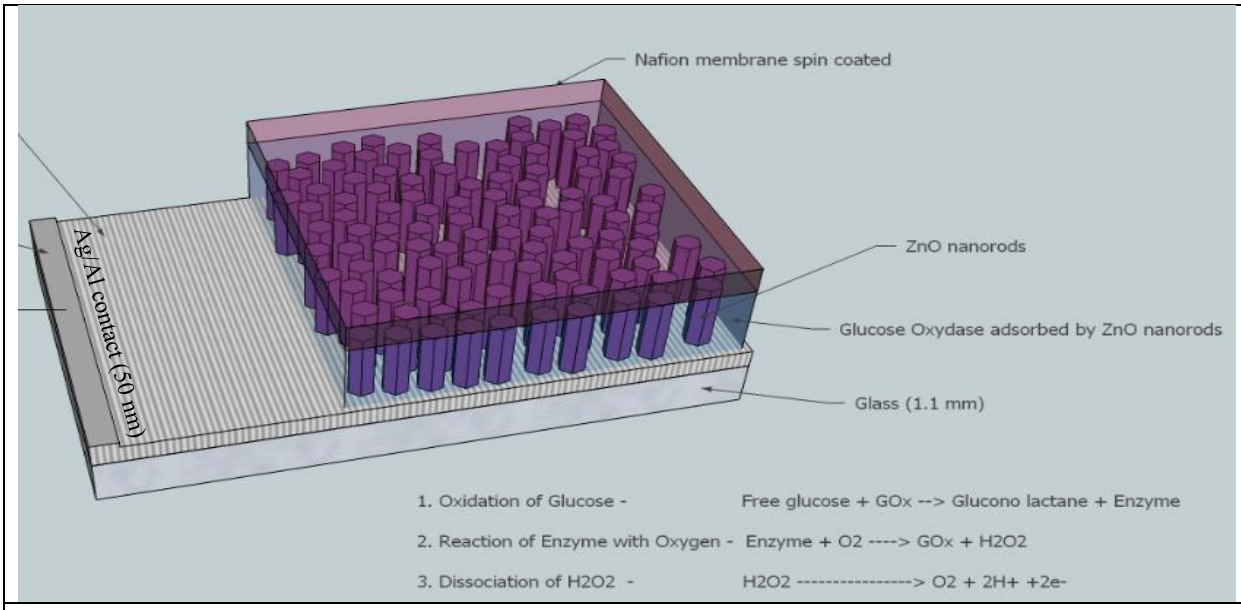

Fig 4: Bio-sensor device unit with ZnO NRs dimensions

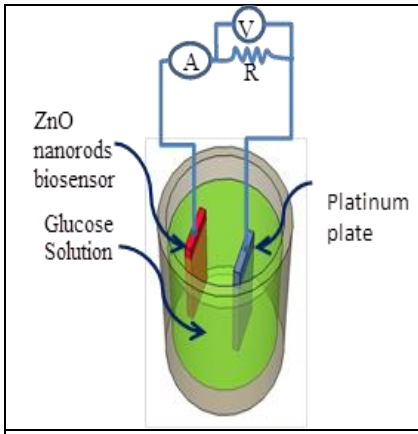

Fig 5: Schematic of test cell showing ZnO biosensor unit and platinum electrode

Figure 5 is a three-dimensional representation of the test cell designed to run the experiment for testing. The test cell consists of glucose as the electrolyte, and a platinum plate as the 2nd electrode and *the immobilized ZnO NRs (adsorbing GOx) as the working electrode*. When a voltage is applied across the two electrodes, electrolysis process takes place. In the process, glucose gets oxidized by GOx to produce an enzyme. This enzyme reacts with oxygen to produce hydrogen peroxide (H_2O_2). Dissociation of hydrogen peroxide gives out electrons into the electrolyte that is detected as sensor sensitivity. The change in the molar concentrations of glucose electrolyte (0.1-20 mM) at a constant voltage determines the sensitivity of the sensor. Here, the term sensitivity can be referred to the change in current with respect to time. Thus, the current in the presence of glucose will be monitored and recorded. Increase in the current indicates the oxidation of glucose to the sensor working electrode (ZnO NRs biosensor).

The output response of a biosensor also depends on factors like pH and temperature that would also be taken under consideration for determining the current vs time output response at different concentrations of glucose electrolyte.

F. Scalable Nanostructured Antireflection Coating for Enhancing Cells Performance:

Nanostructured antireflection coating current progress and limitations: In order to suppress the reflection, several antireflection techniques including subwavelength structures, plasmonic surface, surface passivation, single quarter wavelength, and multilayer coating were investigated. Among all these techniques, subwavelength structures emerged as a successful method due to the characteristics of gradual variation of the refractive index or so called moth-eye effect. The moth-eye effect inspired by the naturally evolved cornea of moth species, which incorporated by nanotip arrays of protuberant structures. A moth eye antireflection surface is one in which the reflection of incident light is reduced by the presence of a regular array of small protuberances covering the surface. Thus, the surface of the moth-eye's provides gradual decrease of refractive index from their cornea to the surrounding medium in order to suppress the reflection of incident light.

Among the antireflective subwavelength structure fabrication methods, the bottom-up deposition is preferable to its top-down counterpart due to simplicity and low cost. Several bottom-up antireflection schemes on GaAs solar cell were reported by using $Si_3N_4/SiO_2/ZnO$ nanorod, indium tin oxide nanocolumns, ZnO nanoneedle, and TiO_2/nanoporous SiO_2. The power conversion efficiency enhancement obtained using these schemes is less than ~ 35 %. Despite superior antireflection properties of the bottom-up schemes, the coupling of multiple discrete layers by a single deposition process is yet to be achieved. For example, previous work fabricated multilayer antireflection coating (ARC) by incorporating either RF sputtering ,oblique angle electron-beam, or chemical deposition in each layer.

Recently, ZnO nanostructure coupled with a single quarter wavelength coating (reflection minimized for a single wavelength) including Si_3N_4, and AZO was substantiated by the other researcher as broadband ARC for the solar cell. A material with refractive index on the order of n ~ 2 such as tantalum pentoxide (Ta_2O_5) can be an alternative for single quarter wavelength coating. Previous investigations on Ta_2O_5 include corrosion protection coating, electrochromic devices, dielectric spacers for metamaterial, and plasmonic coupler. An early attempt by electron beam deposition of a single layer Ta_2O_5 coating on silicon solar cell was reported with an efficiency enhancement on the order of 23 %. However, Ta_2O_5 antireflection coating using sol-gel method limits due to high instability of the sol particle, which originates from fast hydrolysis of tantalum precursor. Therefore, sol stabilization is a crucial parameter for the synthesis of Ta_2O_5 antireflection coating. Moreover, ZnO nanostructure coupled with Ta_2O_5 was not implemented so far, which could provide antireflection characteristics beyond the aforementioned performances.

The broadband suppression in reflection is one of the primary focuses in high efficiency solar cell research. In this project, a moth-eye inspired nanostructure antireflection coating is grown on InAs/GaAs quantum dots solar cell in order to enhance the power conversion efficiency. The abrupt refractive index transition between air and GaAs surface is replaced by a tapering zinc oxide nanoneedle on planar tantalum pentoxide coating. The antireflection structure provides gradual reduction of refractive index away from the solar cell top surface.

Scalable Antireflection Fabrication: The nanostructured antireflection coating is fabricated by utilizing chemical bath deposition of tapered zinc oxide nanoneedles on planar tantalum pentoxide coating. A sol-gel method was developed to obtain an air stable tantalum pentoxide solution. The thickness of the planar tantalum pentoxide coating was optimized to suppress the reflection at a single wavelength. In addition, hydrothermally grown zinc oxide

nanoneedle arrays were optimized by investigating several growth parameters including pH and growth time to obtain a tapered dimension. A tapering zinc oxide nanoneedle structure coupled with a high refractive index tantalum pentoxide layer suppresses the broadband reflectance to less than 1 %.

The combined antireflection structure significantly increased the performance, not only in reflectance or transmission spectrum, but also in current-voltage characteristic, external quantum efficiency, and spectral response measurements. A power conversion efficiency enhancement of 30 % was obtained by a single quarter wavelength tantalum pentoxide layer. Adding the tapered zinc oxide nanoneedles on top of the planar tantalum pentoxide layer, the power conversion efficiency enhanced by 50 %. Furthermore, a 60 % enhancement in the external quantum efficiency is obtained for the same wavelength range.

***Materials growth**:* A sol–gel method of Ta_2O_5 is developed which remains stable in ambient atmosphere. The ZnO nanoneedle arrays were grown by hydrothermal growth method. The bilayer antireflection coating process is shown in details in **Fig. 1**. The pH of the growth solution is adjusted by varying the concentration of diaminopropane (DAP) in the final growth solution in order to obtain the sharp tips as shown in **Fig. 2** (a). The ZnO nanoneedle tip diameter is controlled by increasing growth time. As seen from the Fig. 2 *(b)*, the nanoneedle tip diameter reduced due to the gradual depletion of the zinc nitrate hexahydrate precursors and also the presence of diaminopropane in the growth solution.

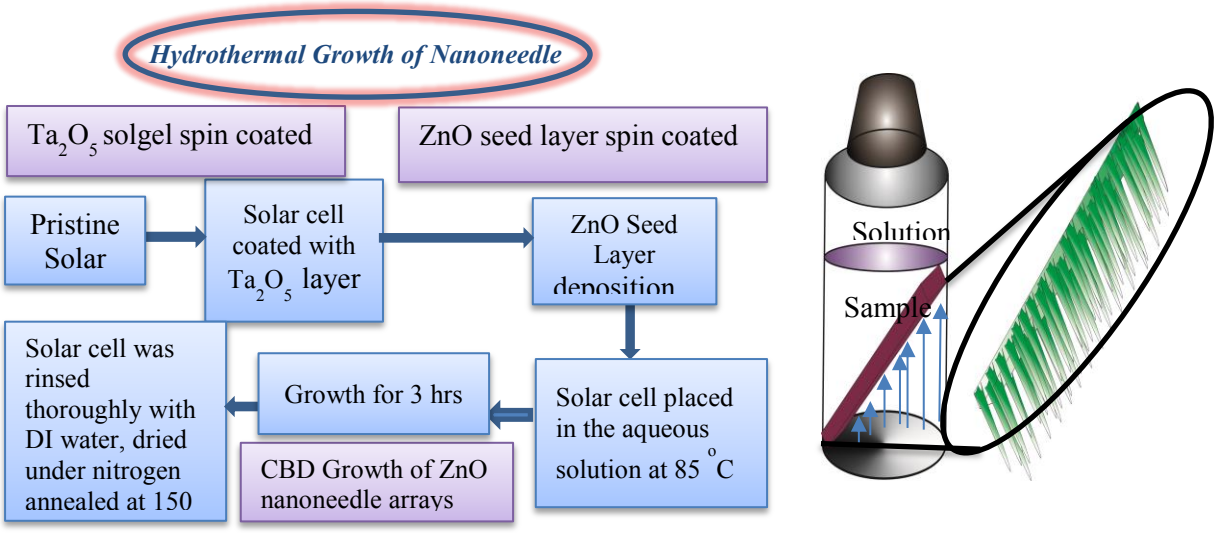

Fig. 1. *Bilayer antireflection coating of ZnO nanoneedle/ Ta_2O_5 fabrication process flow chart.*

***Preliminary Results**:* The structure of InAs/GaAs QDs solar cell is shown in **Fig. 3** *(a)*. In order to compensate the reflection from the GaAs top surface, a novel antireflection structure which consists of a Ta_2O_5 layer and ZnO nanoneedle arrays is utilized as a bilayer antireflection coating. The hierarchical surface texturing of Ta_2O_5 layer and ZnO nanoneedle arrays is shown in Fig. 3 (b) and (c).

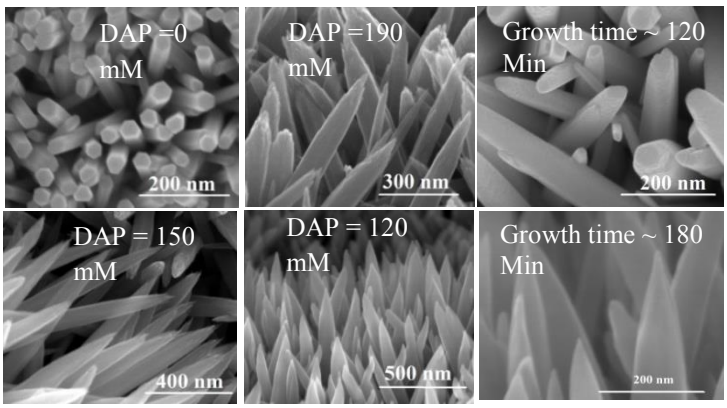

Fig. 2. *Zinc oxide nanoneedle growth parameters*.

The surface morphology of ZnO nanoneedle coupled with Ta_2O_5 (n ~1.9) play a key role in suppressing the reflection by gradual reduction of refractive index away from the GaAs substrate as shown in **Fig. 4** *(a)*. While the incident sunlight impinges on the solar cell from different directions during the day, an omnidirectional ARC is desirable over wide angles of incidence. The average reflectance of ZnO nanoneedle on top of Ta_2O_5 layer is less than 0.6 % over a broad spectral range as shown in Fig. 4 (b). The I-V characteristics of a single layer and a bilayer ARC coatings on InAs QDs solar cells were measured using a four sun AM 1.5 solar simulator as shown in Fig. 4 *(c)*. The bilayer coating showed efficiency (η) enhancement on the order of 50 % from 7.10 % to 10.6 %. The average enhancement in quantum efficiency is on the order of 60 % over the measured spectral range as shown in Fig. 4 *(d)*. The power conversion efficiency of the solar cell enhanced for several reasons. First, the hierarchical surface texturing with high to low refractive index gradient combined with planar Ta_2O_5 coating and ZnO nanoneedle bilayer ARC, decreased reflection to less than 1 %. Second, introduction of Ta_2O_5 with refractive index of 1.9, which is an ideal single layer ARC for GaAs, is given by $\sqrt{n_{GaAs} \times n_{air}}$.

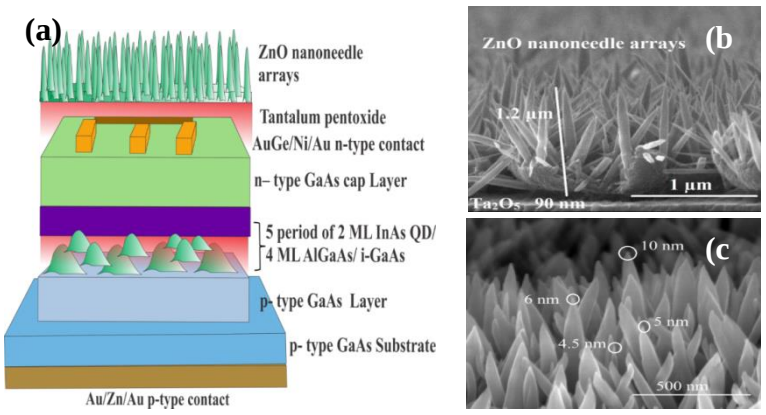

Fig. 3. *a) Schematic diagram of a InAs QDs solar cell with textured surface. b) and c) A representative cross-section and top view of ZnO nanoneedles grown on top of Ta_2O_5.*

The overall performance enhancement obtained by using ZnO nanoneedle/ Ta_2O_5 bilayer coating is better than the performance reported by using different combination of nanostructured surface texturing schemes on GaAs based solar cells. The

significant enhancement compared to other surface texturing approach predominantly originates from the increased photon transmission by the subwavelength dimension ZnO nanoneedle geometry and coupling to a single quarter wavelength Ta_2O_5 coating. The increase in photon transmission leads to a further excitation of electron that increases the generation rate of the photo-excited charge carriers.

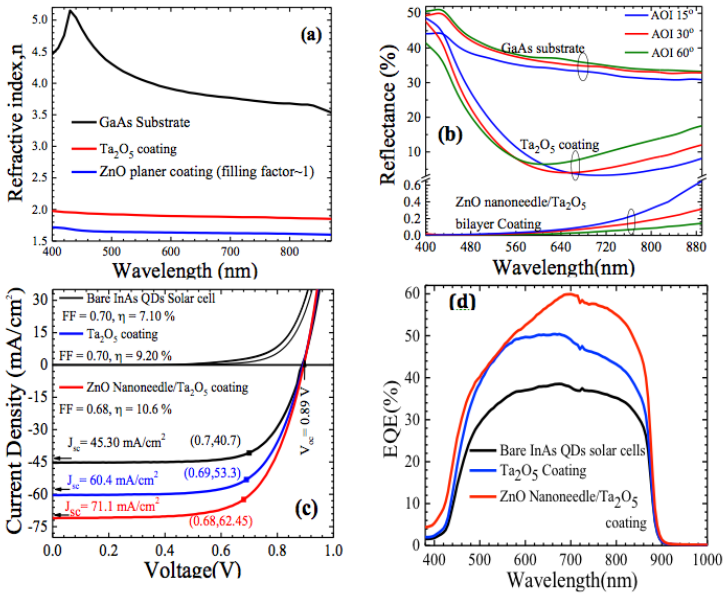

Fig. 4. *a) and b) Refractive index and Reflectance spectra for GaAs substrate with pristine, Ta_2O_5, and ZnO nanoneedles surfaces. c) and d)The I-V characteristics and External quantum efficiency measurement for the InAs QDs solar cell with pristine, Ta_2O_5, and ZnO nanoneedles surfaces.*

All of these preliminary results indicate the research depth that is established by the PIs in the area of solar energy and other optoelectronic devices. The PIs will extend their current research to meet the challenges associated with the prosed research on the two approaches needed for large-scale fabrication. One of the PIs is the president of a local company (Silicon Solar Solution), which is solely devoted to investigate solar cells for mass production. The industrial and government connections established by the PIs throughout the years will definitely help transform the basic research conducted at the University of Arkansas to a level recognized at the industrial national and international levels.